

**Supporting Information for:**

**Ultralight, superelastic and bendable lashing structured nanofibrous  
aerogels for effective sound absorption**

*Leitao Cao,<sup>‡a</sup> Yang Si,<sup>‡a</sup> Yuanyuan Wu,<sup>a</sup> Xueqin Wang,<sup>a</sup> Jianyong Yu<sup>b</sup> and Bin Ding<sup>\*a,b</sup>*

<sup>a</sup> State Key Laboratory for Modification of Chemical Fibers and Polymer Materials, College of Textiles, Donghua University, Shanghai 201620, China

<sup>b</sup> Innovation Center for Textile Science and Technology, Donghua University, Shanghai 200051, China.

**Supporting Information contains:**

Supplementary Methods

Supplementary Discussions

Fig. S1-S21

Table S1-S3

Supplementary References

## Supplementary Methods

### Freeze-drying of fiber dispersions

Generally speaking, the homogenized fiber dispersions were poured into designed molds and frozen by liquid nitrogen to get fast freezing of the samples. The temperature and freezing rate of the sample during the entire freezing process were measured, as showed in Fig. S6a. The different freezing rates were observed with the increase of freezing time, which revealed the phase transition of the water, and the complete freezing of the sample required 10-15 min. Subsequently, the freeze-drying process was performed by using a lyophilizer, as showed in Fig. S6b, it could be observed that the drying curve exhibited a two-step process. Most of the solvent was quickly removed within 15 h and then the remnant crystalline-bounded water required an additional 5-7 h by desorption drying step. After about 22 h, the frozen water was nearly completely removed.

### Determination of the porosity of nanofibrous aerogels

The porosity of prepared aerogels was determined by the following formula:

$$\phi = (V_0 - m / \rho) / V_0 \times 100\% \quad (1)$$

Where  $\phi$  is the porosity,  $V_0$  is the volume,  $m$  is the mass of the solid component, and  $\rho$  is the density of the solid component.

### Measurement of sound absorption properties

The measurements of sound absorption properties were performed at a typical frequency range of 100-6300 Hz using an impedance tube according to ISO 10534-2: 1998. Samples prepared for sound absorption properties measurement were shown in Fig. S17a, the diameters of samples were 100 mm and 30 mm for the frequency of 100-1600 Hz and 1000-6300 Hz, respectively.

Sound absorption properties of the materials have been expressed by sound absorption coefficient  $\alpha$ , which is defined by:

$$\alpha = (E_i - E_r) / E_i \quad (2)$$

Where  $E_i$  is the whole energy of incident sound, and  $E_r$  is the energy of the reflected sound. Fig. S17b showed the schematic of an impedance tube, the transfer function  $H_{12} = P_2 / P_1$  between the two microphones at positions P1 and P2 was measured, and the reflection coefficient was calculated as:<sup>1</sup>

$$r = \frac{H_{12} - e^{-jk_0s}}{e^{jk_0s} - H_{12}} e^{2jk_0L} \quad (3)$$

Where  $s$  is the distance between microphones #1 and #2, and  $L$  is the spacing between microphone #1 and the front surface of the sample.  $j$  is the imaginary unit that  $j^2 = -1$ ,  $k_0$  is the wavenumber which expressed as:  $k_0 = \omega / c_0$ , where  $c_0$  is the speed of sound in air. The absorption coefficient at normal incidence was calculated by:  $\alpha = 1 - |r|^2$ .

### Theoretical calculation

The finite element analysis was conducted as following, a semi-phenomenological JCA model was applied to predict the sound absorption property.<sup>2</sup> JCA model is an equivalent fluid model developed on the basis of Biot theory, and five parameters were required to determine the sound absorption properties of porous materials.<sup>3</sup> porosity  $\phi$ , tortuosity factor  $\alpha_\infty$ , airflow resistivity  $\sigma$ , viscous characteristic length  $\Lambda$  and thermal characteristic length  $\Lambda'$ . The fibers are modelled as infinitely cylinders having a circular cross-section with radius  $r$ .

The tortuosity factor can be approximately expressed as:<sup>4</sup>

$$\alpha_\infty \approx 1 / \sqrt{\phi} \quad (4)$$

In the case of materials with porosity close to 1,  $\Lambda$  and  $\Lambda'$  is given by

$$\Lambda = \frac{1}{2\pi rL} \quad (5)$$

$$\Lambda' = 2\Lambda \quad (6)$$

Where  $L$  is the total length of fibers per unit volume of material,<sup>5</sup> which is calculated as:

$$L = \frac{1}{\pi r^2 (1 - \phi)} \quad (7)$$

The parameters calculated are shown in Table S2.

The effective density  $\rho_{eq}$ , describing the viscous effects, is obtained as:

$$\rho_{eq} = \frac{\alpha_{\infty} \rho_0}{\phi} \left[ 1 + \frac{\sigma \phi}{i \omega \rho_0 \alpha_{\infty}} \sqrt{1 + i \frac{4 \alpha_{\infty}^2 \eta \rho_0 \omega}{\sigma^2 \Lambda^2 \phi^2}} \right] \quad (8)$$

While the bulk modulus  $K_{eq}$ , describing the thermal effects, is predicted as:

$$K_{eq} = \frac{\gamma P_0}{\phi} \left( \gamma - (\gamma - 1) \left( 1 + \frac{8\eta}{i \Lambda'^2 N_{pr} \omega \rho_0} \sqrt{1 + \frac{i \rho_0 \omega N_{pr} \Lambda'^2}{16\eta}} \right)^{-1} \right)^{-1} \quad (9)$$

Where  $\rho_0$  is the density of the air,  $\omega$  is the angular frequency,  $\eta$  is the viscosity of air ( $\sim 1.84 \times 10^{-5}$  Pa s),  $\gamma$  is ratio of the specific heat capacity ( $\sim 1.4$ ),  $P_0$  is the atmospheric pressure ( $\sim 1.01 \times 10^5$  Pa) and  $N_{pr}$  is Prandtl number ( $\sim 0.7$ ).

Based on the above equations, the characteristic impedance  $Z_c$  and wavenumber  $\chi$  are determined as:

$$Z_c = \sqrt{\rho_{eq} K_{eq}} \quad (10)$$

$$\chi = i \omega \sqrt{\rho_{eq} / K_{eq}} \quad (11)$$

The surface impedance  $Z_s$  is calculated as:

$$Z_s = Z_c \coth(\chi d) \quad (11)$$

Where  $d$  is the thickness of sound absorption materials.

The reflection coefficient was calculated as:

$$r = \frac{Z_s - \rho_0 c_0}{Z_s + \rho_0 c_0} \quad (12)$$

Finally, the normal incidence sound absorption  $\alpha$  is calculated by:

$$\alpha = 1 - |r|^2 \quad (13)$$

### Moisture resistance properties of RNFAs

The prepared RNFAs were firstly placed 2~3 cm apart from the mouth of the commercial humidifier for moisture absorption, then left them at an atmosphere of 50~60% RH and a temperature of 20 °C for moisture desorption. The water content was calculated as

$$n = \frac{M_{real} - M_{dry}}{M_{dry}} \times 100\%, \text{ where } M_{dry} \text{ is dry weight of RNFAs and } M_{real} \text{ is the weight when}$$

tested.

Sound absorption properties of RNFAs in various relative humidity were tested as follows: firstly, the dried RNFAs samples were placed in an environment with RH of  $30 \pm 5\%$  for 24 h, then the sound absorption properties were tested. Subsequently, the same samples were put in an environment with RH of  $60 \pm 5\%$  for 24 h, and then the sound absorption properties were tested again. Lastly, the same samples were taken into an environment with RH of  $90 \pm 5\%$  for 24 h, then get the sound absorption data. All the experiments above were performed in an ambient environment with a temperature of 20 °C.

## Supplementary Discussions

### Optimization of the fiber dispersion

The condition of fiber dispersion is a vital factor on the structure construction of RNFA, to ensure the preferable dispersion of microfibers and nanofibers, high molecular weight PAM ( $M_w=10000000$  in this work) was chosen as dispersing additives. Therefore, high viscosity solution could be prepared by using few additives, thus the functions of the fibers will not be affected. Subsequently, we investigated the effect of PAM contents on the viscosity of the solution, and the results showed that the increase of PAM content would lead to higher viscosity (Fig. S3). Furthermore, the stability of PET staple fibers which dispersed in PAM solution was investigated. As was shown in Fig. S4, the PET staple fiber dispersion became stable when PAM content reached 0.1 wt%, because the increase of viscosity decreased the degree of freedom for the fibers, thus the contact and flocculate behavior of dispersed fibers was hindered. In addition, the effect of PAM contents on the morphology of the final RNFA was shown in Fig. S5. With the increase of PAM content in fiber dispersion, the appearance of RNFA became more exquisite. When PAM content in fiber dispersions exceeded 0.1 wt%, the prepared RNFA wrinkled on the surface, which might be caused by the volume shrink of PAM when dried from volume expansive (compare to water solution of PAM) freezing blocks, with more PAM in fiber dispersions, the drag force caused by volume shrink of PAM increased and finally would be reflected on the appearance of prepared RNFA.

### Confirmation of the physical bonding

FTIR characterization of the RNFA before and after heat treatments was showed in Fig. S8a. The peak at  $2242\text{ cm}^{-1}$  indicated the stretching vibration of the  $\text{C}\equiv\text{N}$  band of PAN, the asymmetric absorption peak of C-O-C for PVB was found at  $1124\text{ cm}^{-1}$  and  $1103\text{ cm}^{-1}$ , and

the rocking variation in C-H band of the benzene ring in PET was found at  $723\text{ cm}^{-1}$ . No new peaks appeared in the FT-IR spectrum shown in Fig. S8 after treating RNFAs with  $110^\circ\text{C}$ , suggesting that no chemical reaction took place in the heat-treating process. Thus, the bonding of nanofibers was achieved only by the PVB component in PAN/PVB nanofibers, which would become sticky and gluing the connected fibers together during the heat treating process.

### **Thermal stability of the RNFAs**

Thermal stability and degradation trend of RNFAs and the relative materials were analyzed by TGA. As shown in Fig. S8b, PAN/PVB nanofibers were stable before  $200^\circ\text{C}$  and a quick weight loss was observed at  $270\text{-}300^\circ\text{C}$ , which could be attributed to the decomposition of PVB and partial breakdown of PAN side chains. Moreover, the stage at  $300\text{-}450^\circ\text{C}$  was caused by the cyclization reactions of PAN, and after  $450^\circ\text{C}$  the molecular chain of PAN was broken while a quick decomposition was observed. PET staple fibers showed slight weight loss before  $350^\circ\text{C}$ , indicating relative better thermal stability than PAN/PVB fibers. Comparing with PET and PAN/PVB fibers, the weight loss of RNFAs began at  $\sim 250^\circ\text{C}$ , and the introduction of PET staple fibers endowed the RNFAs with slow weight loss speed, demonstrating that the RNFAs could satisfy the common use in regular temperature, moreover, the slow decomposition speed could avoid the intense structure collapse in high temperature.

### **Comparison of the RNFAs with commercial products**

In order to make the comparison of the sound absorption properties more convincing, commercial melamine foams and nonwoven sound absorption materials were bought for comparison. RNFAs with similar thickness were also made, and all the samples were tested

according to the same standard (ISO 10534-2), detailed comparison was shown in Fig. S19. Although the light weight of commercial melamine foams, their sound absorption properties were fell behind the nonwoven felt and RNFA (Fig. S19a, Fig. S19b), this could be ascribed to the large pore size (about 100~150  $\mu\text{m}$ ) and fewer contact areas (Fig. S19c) of melamine foams. The commercial nonwoven sound absorption felts were made by using microsize fibers (2~30  $\mu\text{m}$ ), the pore size of the nonwoven felts was ranged in tens to hundreds of microns (Fig. S19d), this structure conquered the shortages of the foams in contact areas and tortuosity of the sound pathway, endowing the nonwoven felts better sound absorption properties than melamine foams. However, the weight of the nonwoven felts increased too much. Compared with these materials, the RNFA exhibited advantages both in sound absorption coefficient and reduction of weight. What's more, while keeping the superior sound absorption properties, the obtained RNFA showed nearly half of the density of commercial nonwoven sound absorption felts. Which was attributed to the hierarchal pores structure and large contact area that provided by nanofibers (Fig. S19e).

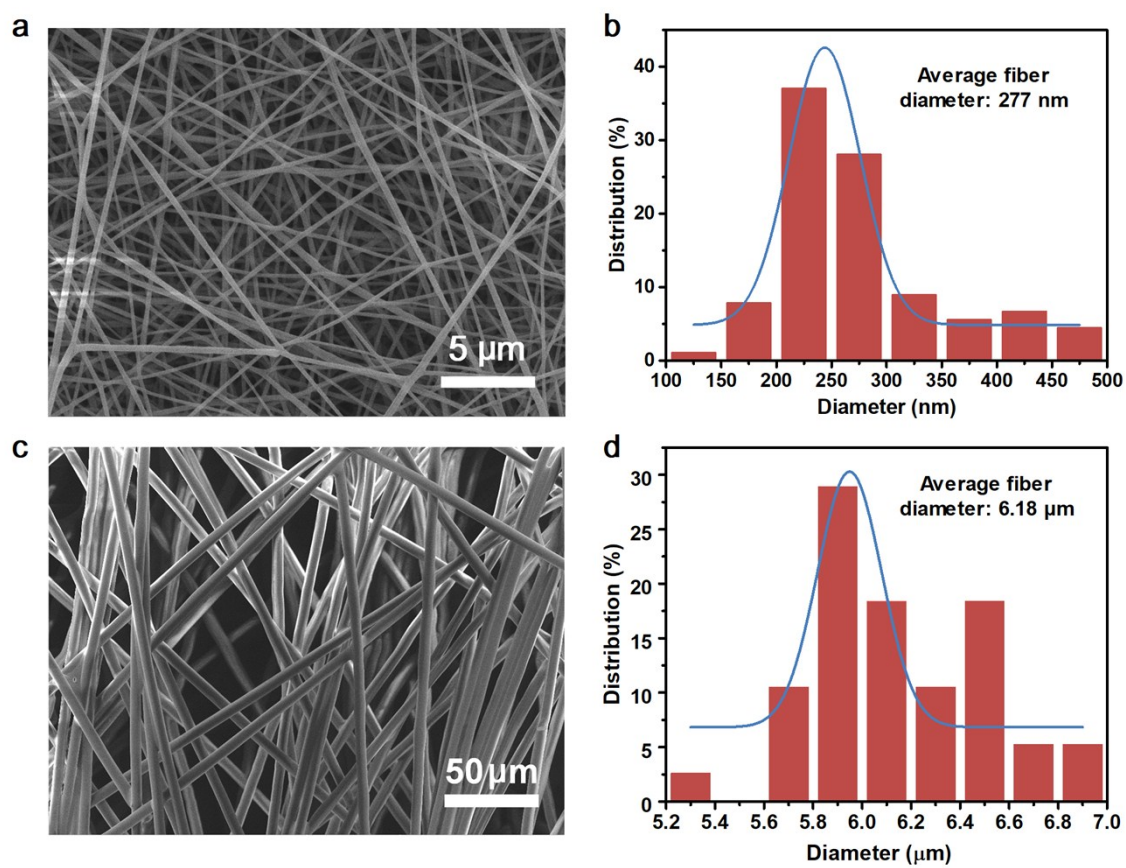


**Fig. S1** Characterization of the raw materials. SEM images of (a) PAN/PVB nanofibers and (c) PET staple fibers. Histogram showing the diameter distribution of (b) PAN/PVB hybrid nanofibers and (d) PET staple fibers.

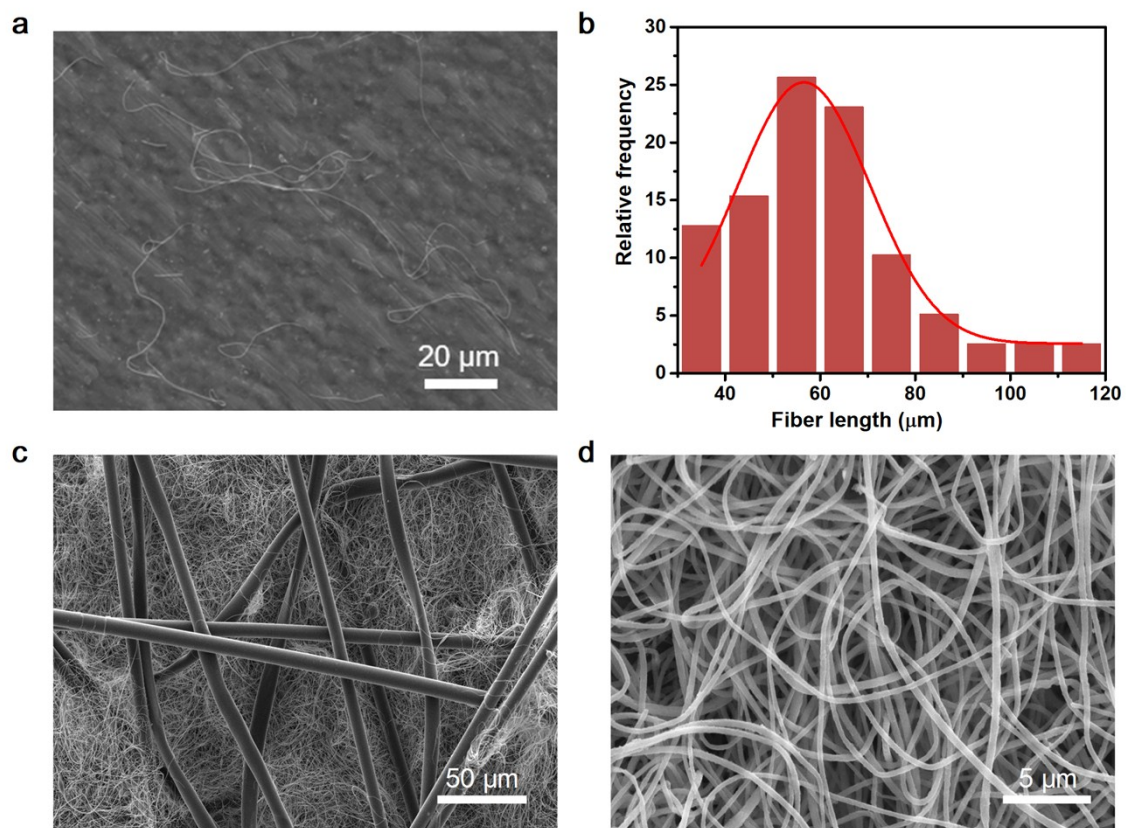


**Fig. S2** Homogenization of the fibers. (a) The SEM image of homogenized PAN/PVB nanofibers and (b) fiber length distribution of the homogenized PAN/PVB nanofibers. (c) SEM images showing the distribution of PET staple fibers and PAN/PVB nanofibers in mixed fiber dispersion. (d) High magnification SEM image for the nanofibers in the dispersion (the SEM samples were prepared by dipping the mixed microfiber and nanofiber dispersions on sample stage without dilution).

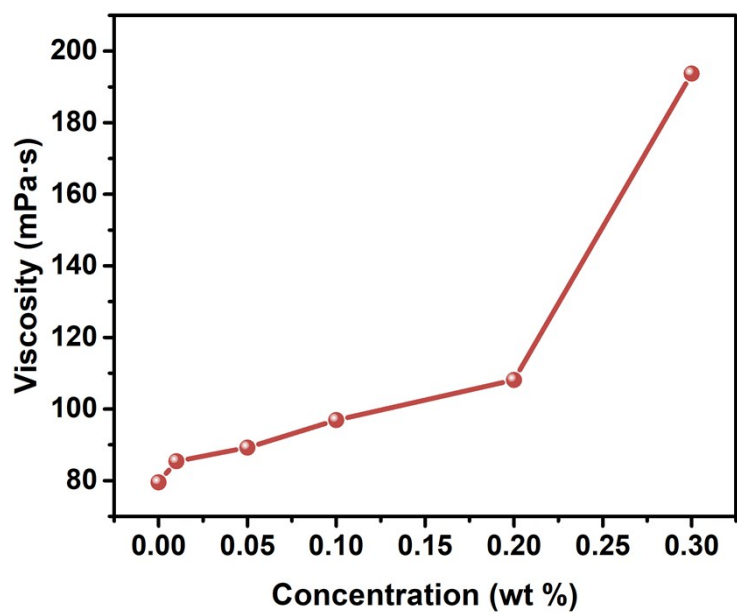


**Fig. S3** Viscosity of the PAM solution. Viscosity of the solution increased with increasing the concentration of PAM from 0 to 0.3 wt%.

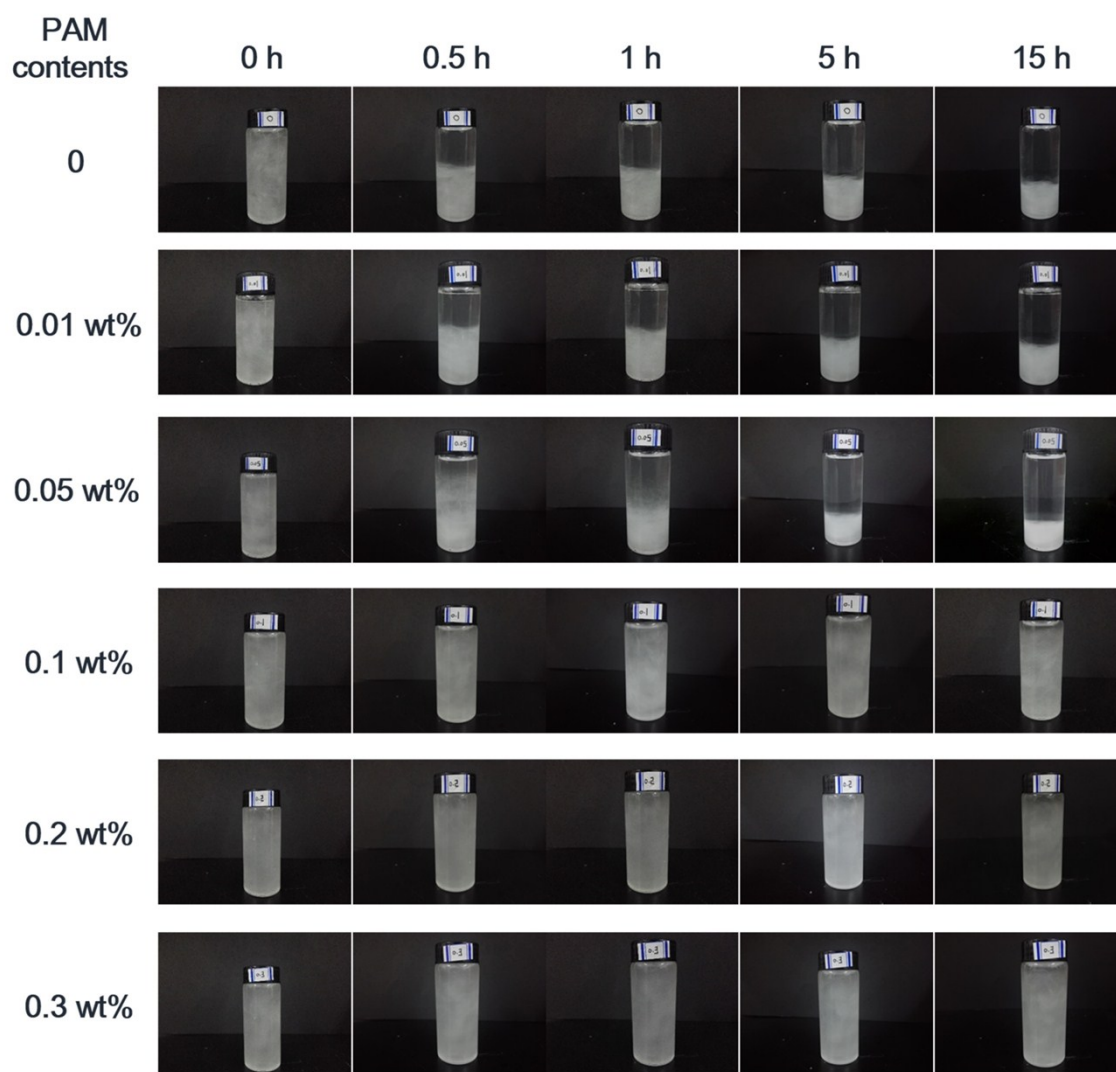


**Fig. S4** Effect of PAM content to the stability of fiber dispersions. The fiber dispersions became stable when the concentration of PAM reached 0.1 wt%.

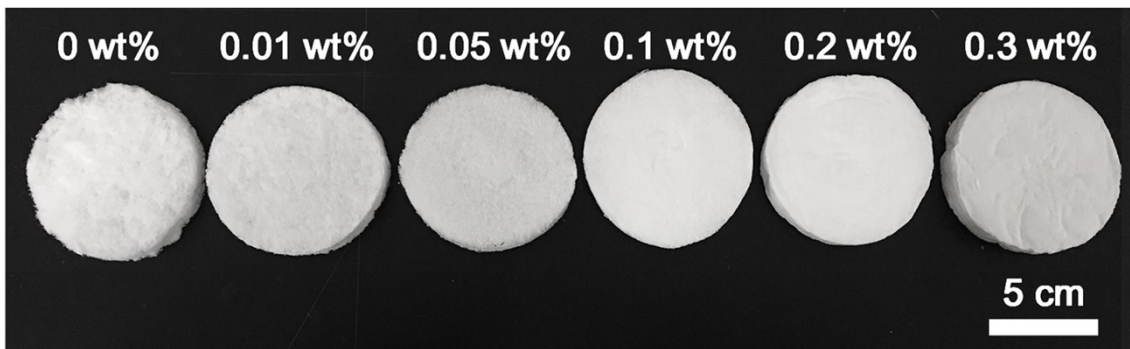


**Fig. S5** Effects of PAM content on the appearance of RNFAAs. Images showing the aerogels made from the fiber dispersions with different contents of PAM, RNFAAs prepared from 0.1 wt% PAM showed relative smooth appearance.

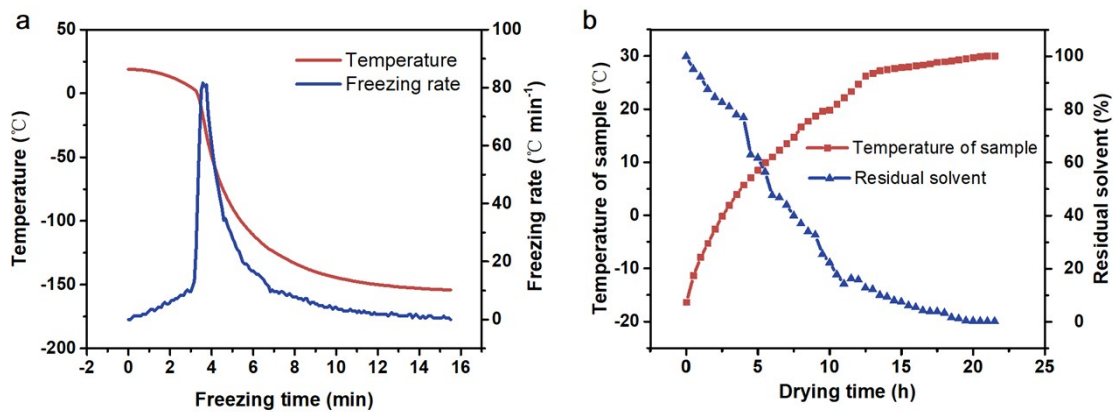


**Fig. S6** The state of dispersions during freeze casting and freeze-drying process. (a) The temperature and corresponding freezing rate of the nanofiber dispersions as a function of freezing time. (b) The changes of the sample temperature and residual solvent with increasing drying time.

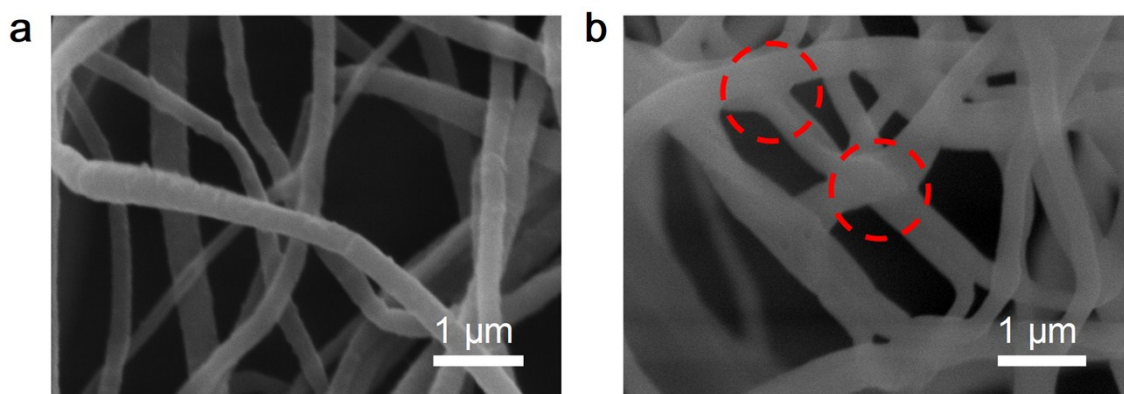


**Fig. S7** The achievement of bonding structure between nanofibers. (a) SEM images showing the condition of PAN/PVB nanofibers in RNFA before heat treatment, the nanofibers were overlapped without bonding. (b) SEM image of the nanofiber network after heat treatment, the overlapped points between nanofibers were bonded by PVB.

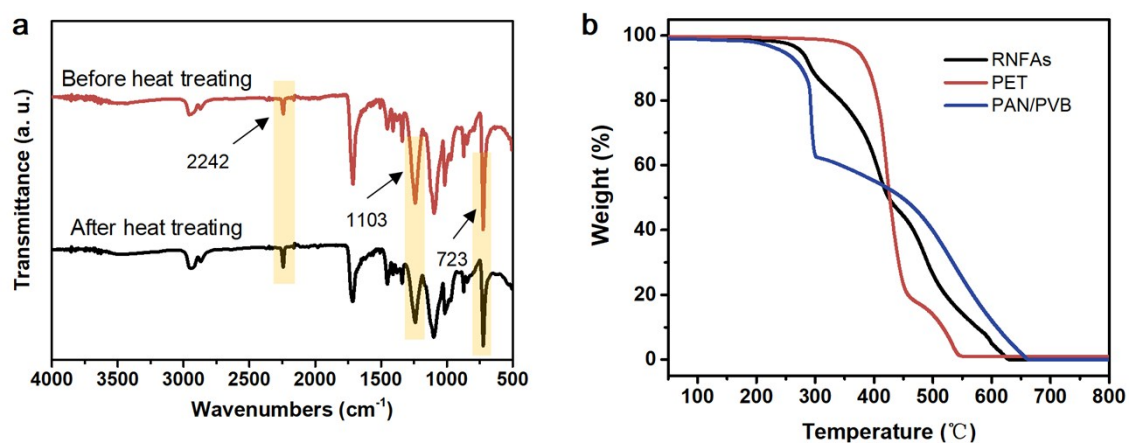


**Fig. S8** Structure confirmation of the RNFA. (a) FT-IR spectra of the RNFA before and after heat treatment. (b) TGA plots of the PET staple fibers, PAN/PVB nanofibers and RNFA.

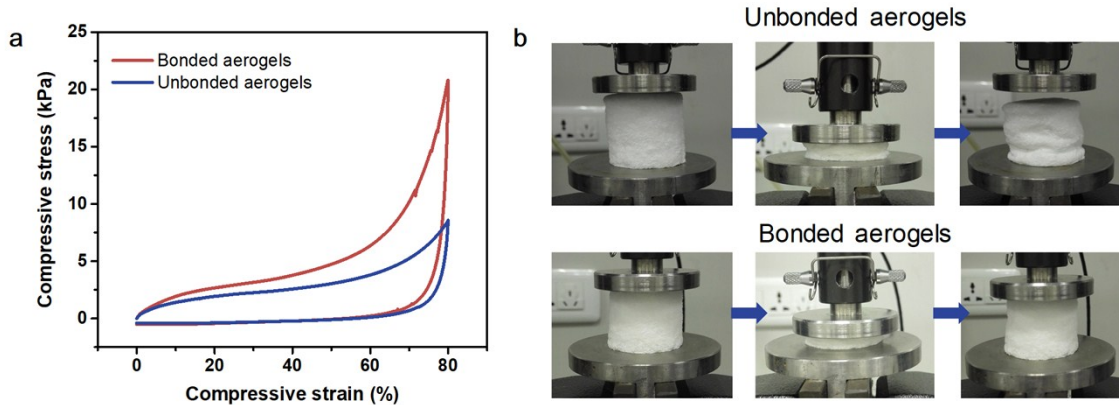


**Fig. S9** Reinforcement of bonding treatment. (a) Compressive curves of the unbonded and bonded fiber aerogels. (b) Demonstration of the improvement in elastic resilience after bonding treatment (density of samples:  $10.76 \text{ mg cm}^{-3}$ ).

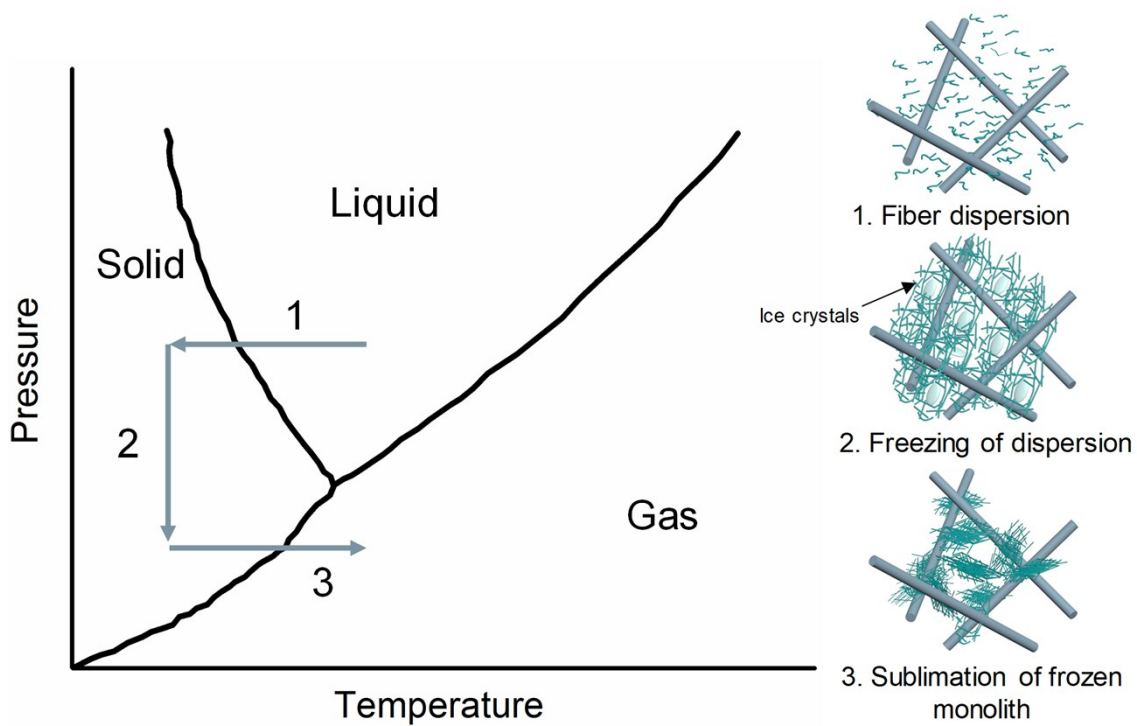


**Fig. S10** Formation mechanism of the hierarchical structure. During the freezing process, nanofibers were rejected by the growth of ice crystals and concentrated between the crystals, the crystals between PET fibers hindered the aggregation of PET staple fibers, then 3D structure was formed after the sample was completely solidified, after freeze-drying, PET staple fibrous frame was formed and interspersed among nanofiber networks as reinforced phase.



**Fig. S11** The RNFAs can be prepared with designed shape by (a) using various molds or (b) directly cutting from large RNFAs felts. (c) The RNFAs can withstand large distortion such as twist.

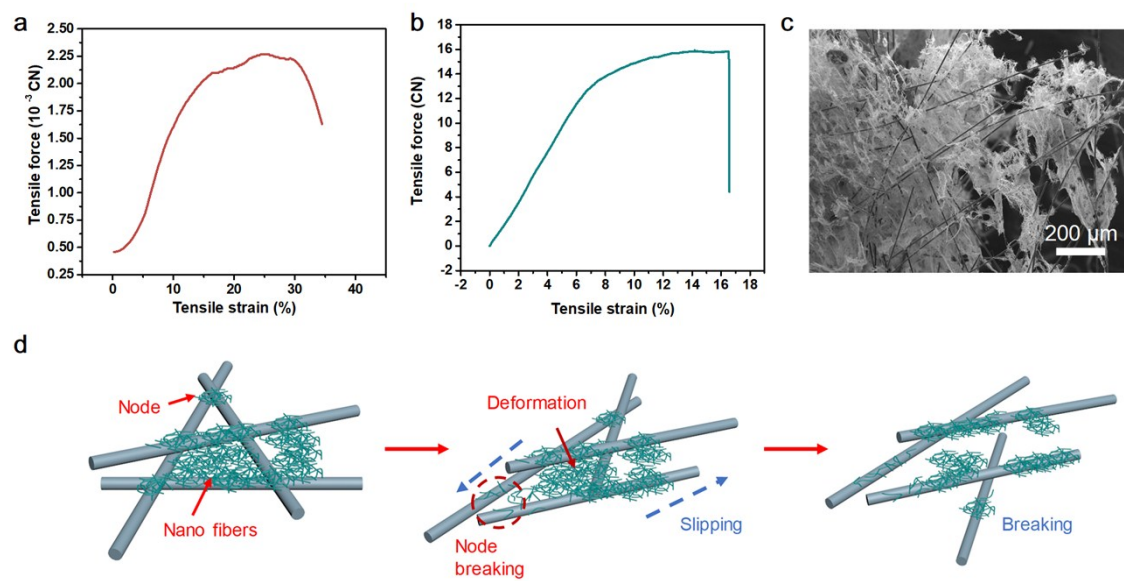


**Fig. S12** Analysis of the tensile properties. Tensile force-strain curves of (a) PAN/PVB hybrid nanofiber and (b) PET staple fiber. (c) The fracture surface of RNFA after tensile failure. (d) Schematic models of the stretching process for RNFA.

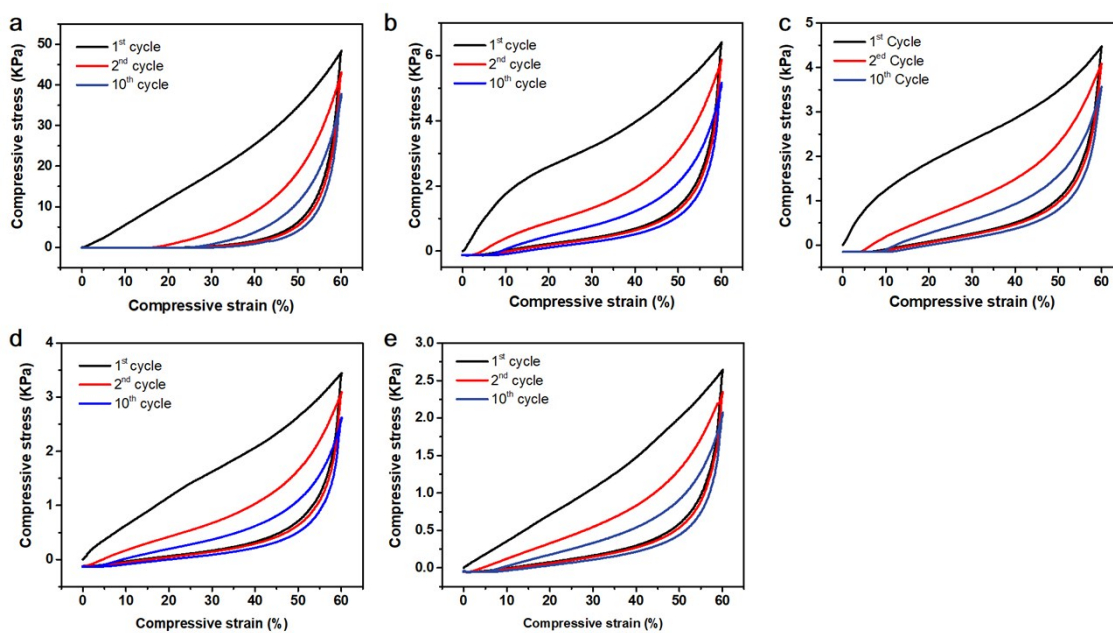


**Fig. S13** Compression properties of fibrous aerogels with different weight contents of microfibers: (a) 0, (b) 40%, (c) 50%, (d) 60% and (e) 70%.

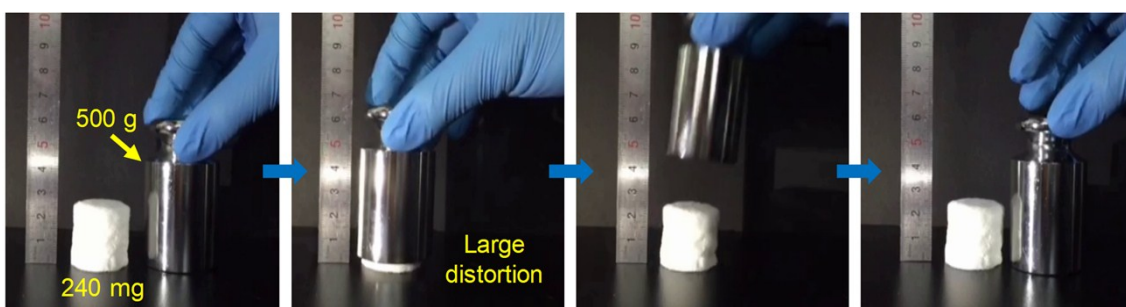


**Fig. S14** Images showing that the RNFA's could quickly recover from large distortion.

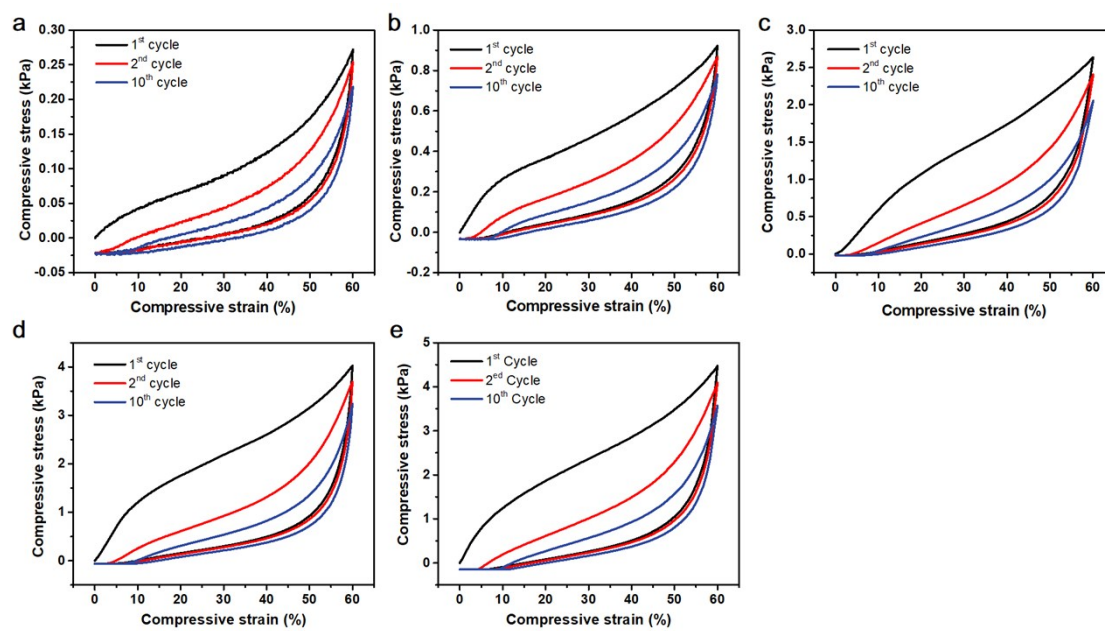


**Fig. S15** Compressive stress-strain curves of the RNFAs with various density of (a) 3.46, (b) 5.02, (c) 7.08, (d) 9.07 and (e) 10.76  $\text{mg cm}^{-3}$ .

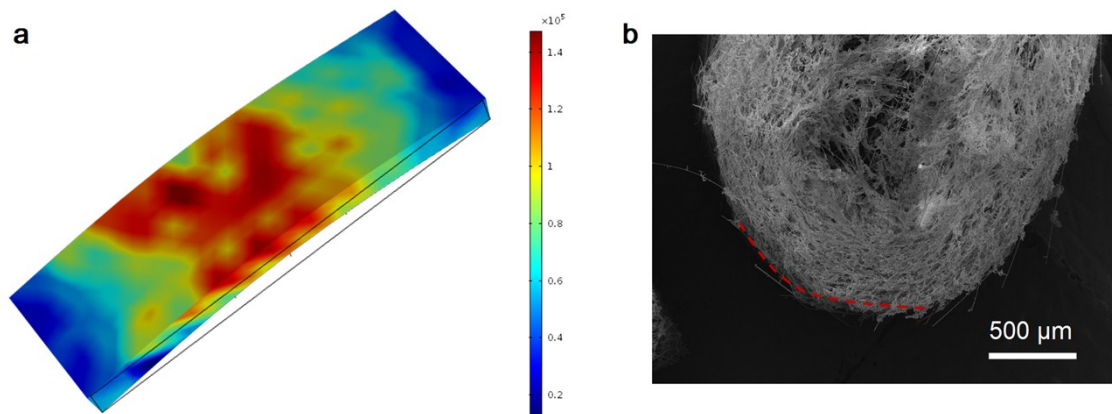


**Fig. S16** Analysis of the bending properties. (a) Image showing the stress distribution of the bent RNFAs. (b) SEM image showing the bent RNFAs.

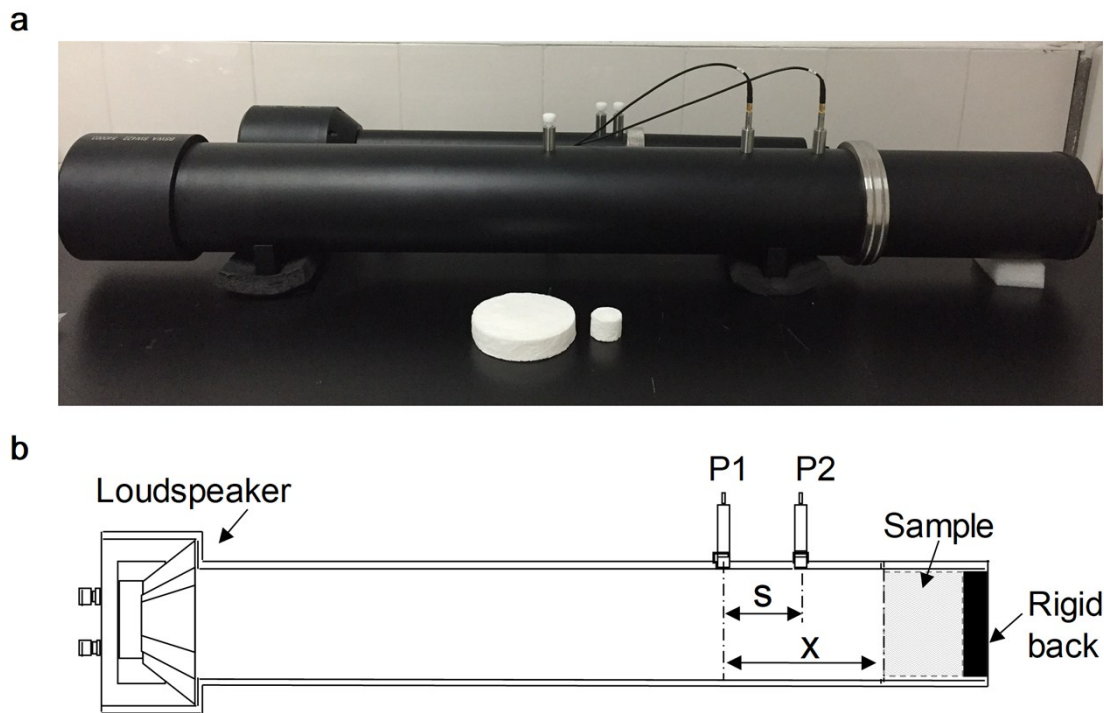


**Fig. S17** Sound absorption testing equipment. (a) Photograph of test samples and the impedance tube. (b) Scheme of the impedance tube.

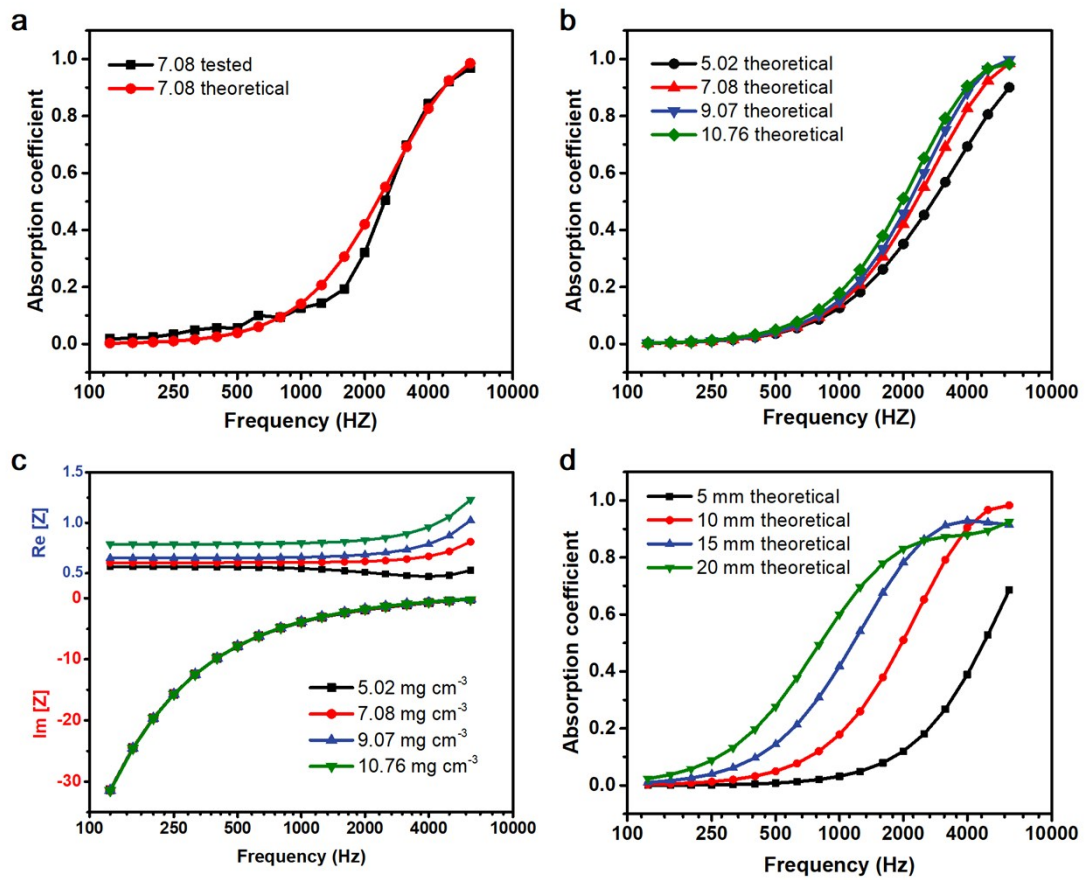


**Fig. S18** Acoustical simulations of RNFA with different density. (a) Comparison of the tested sound absorption coefficient with the one calculated using FEA method. (b) The calculated value of the sound absorption properties and (c) specific surface acoustic impedance of RNFA with various density (thickness of 10 mm, unit of density: mg cm<sup>-3</sup>). (d) Calculated value of the sound absorption properties of RNFA with various thickness (samples with density of 10.76 mg cm<sup>-3</sup>).

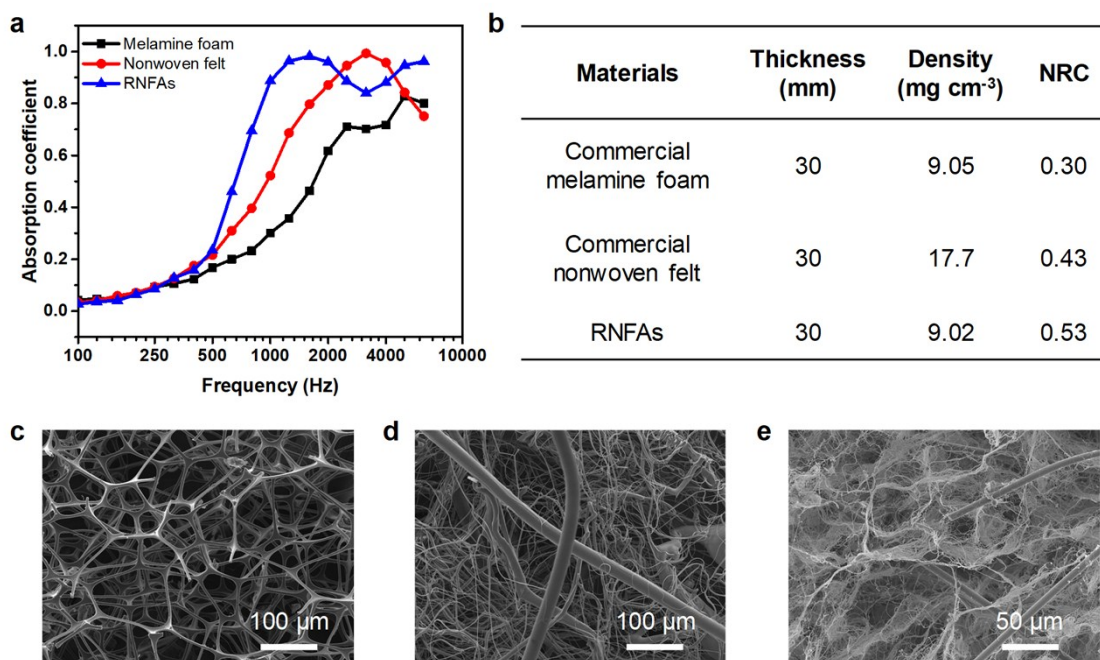


**Fig. S19** Comparison of the various sound absorption materials. (a) Sound absorption properties of commercial melamine foam, commercial nonwoven sound absorption felt and RNFA. (b) The thickness and density of the relative materials. SEM images of (c) commercial melamine foam, (d) commercial nonwoven sound absorption felt, and (e) RNFA.

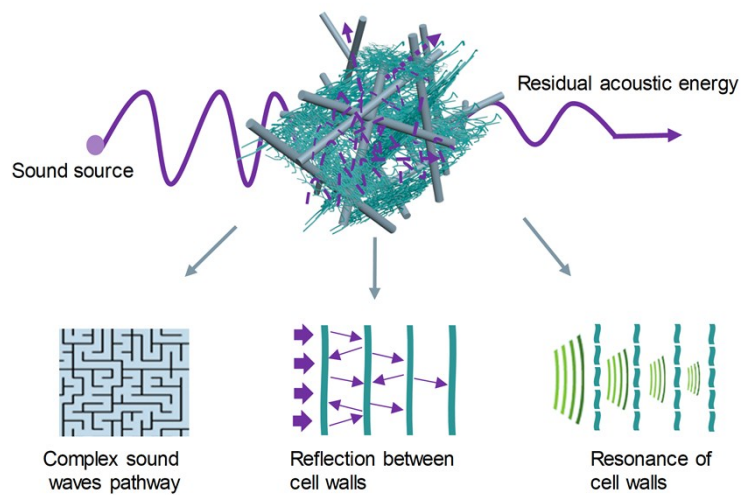


**Fig. S20** Schematic of acoustic propagation through RNFAs. Nanofiber webs in the RNFA offer tortuous pathway for acoustic waves, the cell structure causes the reflection of sound waves between cell walls, and the resonance of cell walls also helped consumed acoustic energy. (Attention should be paid that acoustic wave in air is a longitudinal wave, and the waves and amplitude showed in the schematic is in the purpose to express the energy intensity of acoustic waves.)

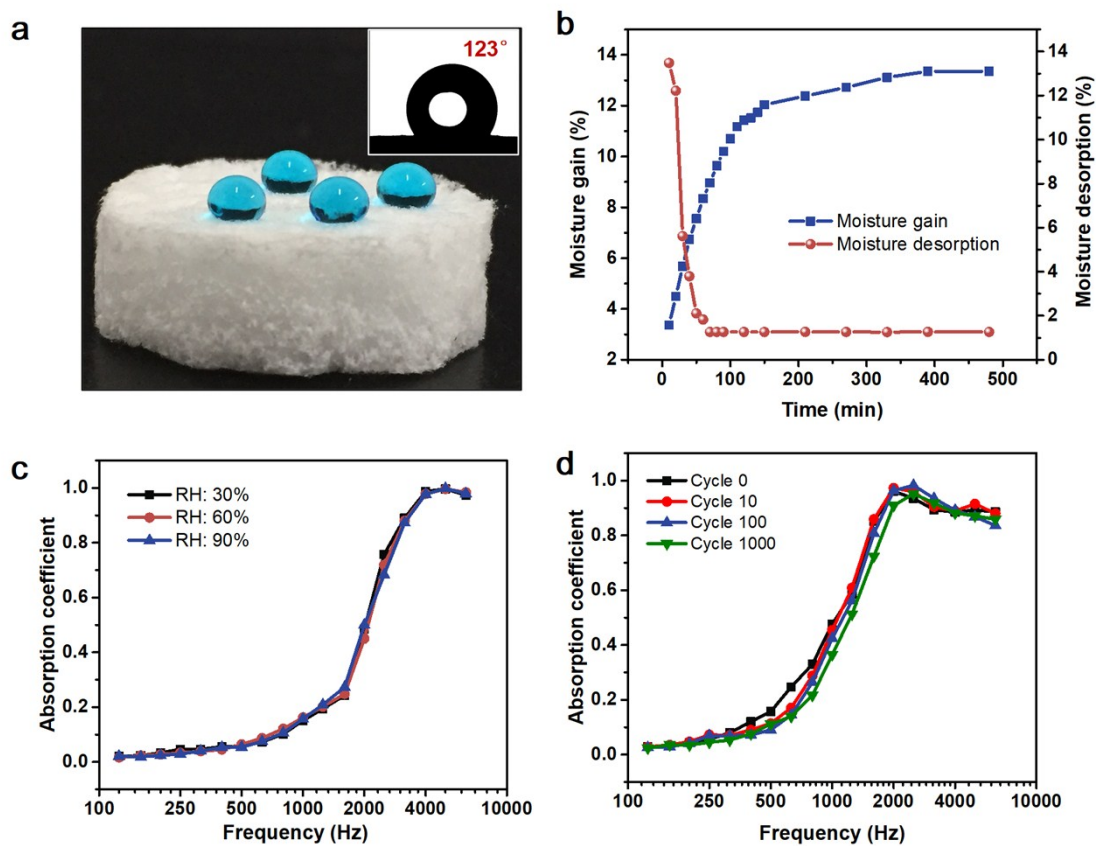


**Fig. S21** Stability of sound absorption performance. (a) Hydrophobic properties of RNFA. (b) Moisture gain and desorption properties of RNFA. (c) Sound absorption properties of RNFA in various RH. (d) Sound absorption properties of RNFA after different compression cycles.

**Table S1.** Recovery ability of various aerogels

<b><i>Constructed Materials</i></b>	<b><i>Density (mg cm<sup>-3</sup>)</i></b>	<b><i>Recovery speed (mm s<sup>-1</sup>)</i></b>	<b><i>Reference</i></b>
<i>PET and PAN/PVB</i>	10.76	834	<i>This work</i>
<i>CNT Arrays</i>	-	2	<i>Nat. Nanotechnol., 2007,2, 417</i>
<i>CNT</i>	5-10	1.2	<i>Adv. Mater., 2010, 22, 617</i>
<i>Graphene-Coated CNT</i>	14	11.2	<i>Nat. Nanotechnol., 2012, 7, 562</i>
<i>Graphene Cellular Monolith</i>	5.1	117	<i>Nat. Commun., 2012, 3, 1241</i>
<i>CNT</i>	122	0.008	<i>Adv. Mater. 2013, 25, 1185</i>
<i>GO-PPy</i>	40	0.2	<i>Adv. Mater. 2013, 25, 591</i>
<i>Cellulose nanocrystals</i>	21.7	1	<i>Chem. Mater. 2014, 26, 6016</i>
<i>Graphene Nanoribbon</i>	9.33	2	<i>Adv. Mater. 2014, 26, 3241</i>
<i>Electrospun Nanofiber</i>	9.6	24	<i>Nat. Commun., 2014, 5, 5802</i>
<i>Cellulose nanocrystal</i>	5.6	0.005	<i>Adv. Mater. 2015, 27, 6104</i>
<i>PAN/SiO<sub>2</sub> nanofiber</i>	17.8	24	<i>ACS Nano, 2015, 9, 3791</i>
<i>C-GO</i>	13.8	580	<i>Nat. Commun., 2016, 7, 12920</i>
<i>Cellulose nanofiber</i>	-	0.2	<i>ACS Nano 2016, 10, 10689</i>
<i>Cellulose</i>	33	0.017	<i>Carbohydr. Polym. 2017, 157, 105</i>

**Table S2.** The parameters of RNFA with various density.

Density ( $\text{mg cm}^{-3}$ )	Porosity (%)	Tortuosity	Thermal characteristic length ( $\mu\text{m}$ )	Viscous characteristic length ( $\mu\text{m}$ )	Flow resistivity ( $\text{Pa s/m}^2$ )
3.46	99.73	1.0014	130	65	19135
5.02	99.6	1.0028	88	44	31845
7.08	99.44	1.0036	63	31	55461
9.07	99.28	1.0043	48	24	69683
10.76	99.14	1.0051	41	20	89764
12.71	99.82	1.006	34	17	12800

**Table S3.** Sound absorption performance and density of various materials.

<b>Material</b>	<b>Density (mg cm<sup>-3</sup>)</b>	<b>Thickness (mm)</b>	<b>NRC</b>	<b>Reference</b>
PAN/PVB and PET	10.76	20	0.41	This work
PAN/PVB and PET	7.08	20	0.37	This work
PET/ silica aerogel	184	30	0.16	<i>Fibers Polym.</i> 2009, 10, 731
Glass fiber	10000	20	0.35	<i>Fibers Polym.</i> 2016, 17, 97.
PET	173	33	0.54	<i>J. Text. I.</i> 2016, 1.
PP	126	12.4	0.27	<i>J. Ind. Text.</i> 2013, 43, 231.
PP and glassfiber	112	13.1	0.19	<i>J. Appl. Polym. Sci.</i> 2012, 123, 2095.
Softwood Kraft pulp	181	11.08	0.19	<i>J. Compos. Mater.</i> 2012, 46, 399.
PLA	94.2	12	0.21	<i>J. Appl. Polym. Sci.</i> 2011, 121, 3056.
PET	112.5	8	0.12	<i>Fiber. Polym.</i> 2010, 11, 782.
Cork	100	30	0.25	<i>Appl. Acoust.</i> 2017, 115, 131.
Luffa fiber		12	0.11	<i>Mater. Lett.</i> 2015, 157, 166.
Wood	260	30	0.20	<i>Build. Environ.</i> 2015, 94, 840.
Coir fiber	825	35	0.30	<i>Acoust. Phys.</i> 2012, 58, 246

## Supplementary References

1. G. Amaral-Labat, E. Gourdon, V. Fierro, A. Pizzi and A. Celzard, *Carbon*, 2013, **58**, 76-86.
2. B. Botterman, G. C. H. D. de la Gree, M. C. J. Hornikx, Q. L. Yu and H. J. H. Brouwers, *Appl. Acoust.*, 2018, **129**, 144-154.
3. X. H. Yang, S. W. Ren, W. B. Wang, X. Liu, F. X. Xin and T. J. Lu, *Compos. Sci. Technol.*, 2015, **118**, 276-283.
4. M. Ayub, M. J. M. Nor, M. H. Fouladi, R. Zulkifli and N. Amin, *Acoust. Phys.*, 2012, **58**, 246-255.
5. J. Allard and N. Atalla, *Propagation of sound in porous media: modelling sound absorbing materials 2e*, John Wiley & Sons, 2009.